AGU ADVANCING EARTH AND SPACE SCIENCE

JGR Space Physics

RESEARCH ARTICLE
10.1029/2020JA028988

Key Points:

- A one-dimensional radial diffusion model driven by solar wind parameters is developed to simulate the dynamics of radiation belt electrons
- The variations of radiation belt electrons from 2012 to 2015 are simulated and compared with satellite observations at $L = 5$ and at $L = 4$
- The solar wind speed is more likely to influence electron flux at higher L while dynamic pressure has more influence on electrons at lower L

Correspondence to:
Z. Xiang,
xiangzheng@whu.edu.cn

Citation:
Xiang, Z., Li, X., Kapali, S., Gannon, J., Ni, B., Zhao, H., et al. (2021). Modeling the dynamics of radiation belt electrons with source and loss driven by the solar wind. *Journal of Geophysical Research: Space Physics*, *126*, e2020JA028988. https://doi.org/10.1029/2020JA028988

Received 30 NOV 2020
Accepted 8 MAY 2021

Modeling the Dynamics of Radiation Belt Electrons With Source and Loss Driven by the Solar Wind

Zheng Xiang[1,2], Xinlin Li[2,3], Sudha Kapali[4], Jennifer Gannon[4], Binbin Ni[1,5], Hong Zhao[2,6], Kun Zhang[2,3,7], and Leng Ying Khoo[2,3]

[1]Department of Space Physics, School of Electronic Information, Wuhan University, Wuhan, Hubei, China, [2]Laboratory for Atmospheric and Space Physics, University of Colorado Boulder, Boulder, CO, USA, [3]Department of Aerospace Engineering Sciences, University of Colorado Boulder, Boulder, CO, USA, [4]Computational Physics, Inc., Boulder, Colorado, USA, [5]CAS Center for Excellence in Comparative Planetology, Hefei, Anhui, China, [6]Physics Department, Auburn University, Auburn, AL, USA, [7]Space Science Institute, Boulder, CO, USA

Abstract A radial diffusion model directly driven by the solar wind is developed to reproduce MeV electron variations between $L = 2$–12 (L is L^* in this study) from October 2012 to April 2015. The radial diffusion coefficient, internal source rate, quick loss due to EMIC waves, and slow loss due to hiss waves are all expressed in terms of the solar wind speed, dynamic pressure, and interplanetary magnetic field (IMF). The model achieves a prediction efficiency (PE) of 0.45 at $L = 5$ and 0.51 at $L = 4$ after converting the electron phase space densities to differential fluxes and comparing with Van Allen Probes measurements of 2 and 3 MeV electrons at $L = 5$ and $L = 4$, respectively. Machine learning techniques are used to tune parameters to get higher PE. By tuning parameters for every 60-day period, the model obtains PE values of 0.58 and 0.82 at $L = 5$ and $L = 4$, respectively. Inspired by these results, we divide the solar wind activity into three categories based on the condition of solar wind speed, IMF Bz, and dynamic pressure, and then tune these three sets of parameters to obtain the highest PE. This experiment confirms that the solar wind speed has the greatest influence on the electron flux variations, particularly at higher L, while the dynamic pressure has more influence at lower L. Also, the PE at $L = 4$ is mostly higher than those at $L = 5$, suggesting that the electron loss due to the magnetopause shadowing combined with the outward radial diffusion is not well captured in the model.

1. Introduction

The dynamics of relativistic electrons in the Earth's magnetosphere are of fundamental science interest and of considerable practical importance because of their effect on spacecraft and because of their radiation hazard to astronauts who perform extravehicular activity (EVA) (e.g., Baker, 2001; Baker, Allen et al., 1998; Fennell et al., 2001). A real-time prediction model of radiation belt electron flux can provide operators time to mitigate these hazards and help to reveal the underlying physical mechanisms of electron dynamics (e.g., Li, 2004; Boynton et al., 2013, 2016).

The outer electron radiation belt is the product of warm plasma transporting into the inner magnetosphere during magnetic storms. Plasmas waves and magnetic field re-configurations play key roles in the variability of the outer belt electrons. Lower energy electrons (<20 keV) are transported rapidly inward from the magnetotail into the inner magnetosphere by convective electric fields during magnetic storms (e.g., Li et al., 2009; Jaynes et al., 2015). For electrons with higher energies, radial diffusion, a slower process involving many individual fluctuations of fields, may dominate the transport (e.g., Zhao, Baker, et al., 2019). Lower energy electrons that have been rapidly transported into the inner magnetosphere can then be energized in situ by plasma waves outside the plasmasphere, or radial diffusion can energize electrons by transporting them inward from the outer part of magnetosphere to the inner magnetosphere. However, the relative role of these two processes is not well understood. Recently the paradigm for explaining the creation of the electron radiation belt has shifted from the almost exclusive use of the theory of radial diffusion to greater emphasis on the role of waves in the in-situ heating of radiation belt electron (e.g., Boyd et al., 2018; Li et al., 1999; Reeves et al., 2013). The waves are a direct consequence of the injection of plasmasheet electrons into the inner magnetosphere (Chen et al., 2007; Horne et al., 2005; Shprits, Thorne, Horne et al., 2006). These electrons generate strong chorus whistler

waves, which can both scatter electrons into the loss cone and heat lower energy electrons outside the plasmasphere to produce a high energy tail on the electron distribution, creating the outer radiation belt. Satellite observations (e.g., Baker, Pulkkinen et al., 1998; Li et al., 2006; X. Li et al., 2017; Zhao & Li, 2013; Zhao et al., 2018) suggest the following scenario for the creation of the electron radiation belt: during magnetic storms, plasma convection penetrates deeper into the magnetosphere, replacing the cold plasma in the outer plasmasphere with warm plasma in energy range up to 10s of keV. The pre-existing outer belt electrons are scattered and lost by plasma waves generated by the newly injected warm electrons. Simultaneously a new radiation belt begins to form in the region outside of the eroded plasmasphere by some combination of in-situ heating of the newly injected warm electrons and radial transport of energetic electrons from further out.

During active times, both magnetopause shadowing followed by outward radial diffusion and atmospheric precipitations due to wave-induced pitch angle diffusion play important roles in the loss of radiation belt electrons (e.g., Li et al., 1997; Ma et al., 2020; Morley et al., 2010; Tu et al., 2010; Turner et al., 2012; Xiang et al., 2016). The inward movement of the magnetopause due to strong solar wind dynamic pressure (P_{dyn}) can substantially deplete electrons at high L shells where electrons find themselves on open drift shells, which is called magnetopause shadowing (e.g., Shprits, Thorne, Friedel et al., 2006). The other important loss mechanism of electrons is diffusion induced by magnetospheric waves, including chorus waves, plasmaspheric hiss, and electromagnetic ion cyclotron (EMIC) waves (e.g., Ni et al., 2013; 2015; 2017; Summers et al., 2007; Thorne, 2010; Turner et al., 2014). During quiet periods, hiss waves play an important role in the loss of radiation belt electrons inside the plasmasphere (Abel & Thorne, 1998; Breneman et al., 2015; Fu et al., 2020; Ni et al., 2013; Zhang et al., 2018; 2019) and produce a reversed electron energy spectrum in the plasmasphere (Ni et al., 2019; Zhao, Johnston et al., 2019; Zhao, Ni et al., 2019). During active times, EMIC waves can lead to significant decrease of electrons in a few minutes due to cyclotron resonance or bounce resonance (e.g., Blum et al., 2015; Xiang et al., 2017, 2018).

In this study, we build a model incorporating the above source and loss mechanisms to reproduce satellite observations of MeV electron at different L values. The model has realistic boundary conditions at the plasmapause and magnetopause and uses real-time solar wind parameters as the input (e.g., Balikhin et al., 2011, 2016; Li et al., 2001). The free parameters in the model are optimized through machine learning techniques. This model can make predictions of the electron flux in advance since enhancements of electron flux follow solar wind speed enhancement (e.g., Li et al., 2011; Paulikas & Blake, 1979). The descriptions of each term in the model are provided in Section 2. We present the simulation results in Section 3 and summarize the results in Section 4.

2. Model Description

Our model uses the one-dimensional (1-D) radial diffusion Fokker-Planck equation (Schulz & Lanzerotti, 1974):

$$\frac{\partial f}{\partial t} = L^2 \frac{\partial}{\partial t}\left(\frac{D_{LL}}{L^2}\frac{\partial f}{\partial L}\right) - \frac{f}{\tau} + S, \tag{1}$$

where f is the electron phase space density (PSD), L is L^* but we drop the asterisk here and for the rest of the equations in this paper, D_{LL} is radial diffusion coefficient, τ is the electron lifetime, and S is the source rate due to heating. The D_{LL}, τ, and S are all expressed with solar wind parameters.

For the radial diffusion rate, we adopt the empirical formula from Li et al. (2011):

$$D_{LL} = D_0\left(\frac{L}{6.6}\right)^{10}, \tag{2}$$

$$D_0 = C_1\left(\frac{v}{v_0}\right)^{\gamma 1}\left[1+\left(\frac{v_x b_z + |v_x b_z|}{\alpha_1}\right)^2\right]^{\gamma 2}\left[\frac{\left(\Delta v^2 / \Delta t\right)^2}{\beta}\right]^{\gamma 3}, \quad (3)$$

where the first term is a function of the solar wind velocity (v) divided by its average (v_0) value of, as calculated from October 2012 to April 2015, 375 km/s; the second term is a function of the y-component of solar wind electric field, v_x is the x component of the solar wind speed while b_z is the z component of the interplanetary magnetic field (IMF) in, GSM coordinate; the third term is a function of solar wind velocity fluctuations, $\Delta v^2 / \Delta t$ is directly calculated from the solar wind speed using data at a rate of one measurement every 10 min and β is the average of $\Delta v^2 / \Delta t$. The definition of velocity fluctuation follows Li et al. (2001), which is an approximation of $2v\left(dv / dt\right)$, a combination of solar velocity and velocity fluctuation.

The magnetopause standoff position is calculated by Shue et al. (1998):

$$r_0 = \left(10.22 + 1.29 \times \tanh\left(0.184 \times \left(b_z + 8.14\right)\right)\right)\left(P_{\text{dyn}}\right)^{-1/6.6} + \Delta L_1, \quad (4)$$

where P_{dyn} is solar wind dynamic pressure, ΔL_1 represents some uncertainties in the magnetopause model of Shue et al., (1998). Outside the magnetopause, the electron lifetime is set to a low value, for example, 0.02 days, since, outside the magnetopause, the electrons will not be trapped by the Earth's magnetic field and experience a sudden decrease. Thus, we set the electron lifetime outside the magnetopause to a low value comparable to the electron drift period, usually ranges in minutes (e.g., 0.02 days ≈ 30 min).

The plasmapause position is calculated by Verbanac et al. (2015):

$$L_{\text{pp}} = -0.373 \times B \times v + 5.96 + \Delta L_2, \quad (5)$$

where B is the interplanetary magnetic field strength, ΔL_2 represents some uncertainties in the plasmapause model.

Outside the plasmasphere, we consider electron acceleration from chorus wave using a formula like the form of radial diffusion rate:

$$S = C_2\left(\frac{v}{v_0}\right)^{\gamma 4}\left[1+\left(\frac{v_x b_z + |v_x b_z|}{\alpha_2}\right)^2\right]^{\gamma 5} w\left(L\right), Lpp < L < Lpp + \Delta L_3, \quad (6)$$

$$w\left(L\right) = \frac{0.2}{|L - L_0| + 0.1}, \quad (7)$$

where $w(L)$ represents the L dependence of heating rate S, we set $L_0 = 4.4$ since the peaks of radial profile of MeV electrons are generally around $L = 4$ (e.g., Reeves et al., 2013). Since the electrons outside the magnetopause are set with short lifetime, the enhancement of electron PSD in the simulation are controlled by the term S. Namely, we assume the in situ heating rather than inward radial diffusion is the main source mechanism right outside the plasmapause. ΔL_3 defines a finite region of local heating.

Losses inside the plasmasphere are mainly caused by resonance with plasmaspheric hiss. Orlova et al. (2016) built a new global loss model of energetic and relativistic electrons based on hiss wave measurements from the Van Allen Probes. We use Equation 3 of Orlova et al. (2016) to calculate lifetime of electrons inside plasmasphere:

$$\tau\left(L, E, Kp\right) = \frac{\tau_{av}\left(L, E\right)}{h\left(Kp\right)}, L < L_{\text{pp}}, \quad (8)$$

where E is electron energy. The formula of $\tau_{av}(L,E)$ can be found in Orlova et al. (2016). The term $(h(Kp) = (1/1315)10^{-0.01414Kp^2+0.2321Kp+2.598}$ in Orlova et al., 2016) has been revised to relate with solar wind parameters rather than Kp index:

$$h(Kp) = C_3\left(\frac{v}{v_0}\right)^{\gamma_6}\left[1+\left(\frac{v_x b_z + |v_x b_z|}{\alpha_3}\right)^2\right]^{\gamma_7}, \quad (9)$$

The relationship between first adiabatic invariants μ (MeV/G) and electron energy E (MeV) is expressed as (Tu et al., 2009):

$$E = \sqrt{0.512^2 + 0.307\mu L^{-3}} - 0.512 \quad (10)$$

The quick loss due to EMIC wave near plasmapause is also related to solar wind parameters as:

$$\tau(\mathrm{EMIC}) = C_4\left(\frac{P_{\mathrm{dyn}}}{P_{\mathrm{dyn}_0}}\right)^{\gamma_8}\left[1+\left(\frac{v_x b_z + |v_x b_z|}{\alpha_4}\right)^2\right]^{\gamma_9}, \quad L_{\mathrm{pp}} - \Delta L_4 < L < L_{\mathrm{pp}} + \Delta L_4, \quad (11)$$

This term only takes effect when the value of solar wind dynamic pressure is greater than 7 nPa since EMIC wave excitation mostly correlates to high solar wind dynamic pressure (Lessard et al., 2019; Saikin et al., 2016). The 7 nPa is an empirical value from simulation results (Chen et al., 2020). The loss effect due to chorus waves is not induced in the model, since chorus waves mostly scatter tens of keV electrons and have slight effect on the loss of MeV electrons (Ni et al., 2008, 2011). ΔL_4 defines a finite region of quick loss near the plasmapause.

To summarize, the free parameters in our model are scaling factors C_1–C_4, space width factors ΔL_1–ΔL_4, and factors adjusting the contribution of various solar wind parameters $\gamma_1 - \gamma_9$, $\alpha_1 - \alpha_4$. Here, the free parameters are those which can be adjusted in a reasonable range in the model to obtain the best prediction of the satellite measurements. Similar form is used in Equations 6, 9, and 11 to link loss or source terms with solar wind parameters since magnetosphere variability is mostly driven by the variability of the solar wind. IMF Bz and solar wind speed are critical for electron acceleration to >1 MeV energies in the heart of the outer radiation belt (Li et al., 2015; Reeves et al., 2011) and often used to predict Kp index (Ji et al., 2013; Wing et al., 2005). Thus, solar wind velocity and IMF Bz are used in Equations 6 and 9. Similarly, solar wind dynamic pressure and IMF Bz are related to EMIC wave distribution and used in Equation 11 (Saikin et al., 2016).

In the model, the outer boundary is $L = 12$ while the inner boundary is $L = 2$. The outer boundary is determined based on the last closed drift shell or the magnetopause location (Shue et al., 1998; Xiang et al., 2017). The inner boundary is associated with the slot region where electron fluxes generally stay at low levels (X. Li et al., 2017). There are 100 grid points in L and the time step is 10 min. The model performance was measured by the prediction efficiency (PE) (Li, 2004; Li et al., 2001) and the linear correlation (LC) coefficient over the defined interval. PE is defined as:

$$\mathrm{PE} = 1 - \frac{\text{mean square residual}}{\text{variance of data}} = 1 - \frac{\sum_i^n (d_i - p_i)^2}{\sum_i^n (d_i - \bar{d})^2}, \quad (12)$$

where d_i and p_i are the data and model results, respectively, and $\bar{d}$ is the mean of all d_i. $PE = 0$: model results are as good as the averaged data; PE > 0: the model is better than reproducing the average and PE = 1: perfect modeling.

In this study, the algorithm of Bayesian optimization using Gaussian processes are used to find the highest PE and the corresponding free parameter values (Frazier, 2018; Rasmussen & Wilians, 2006). This idea is to optimize the PE of the radiation belt model using Gaussian process regressions, that is, the PE values are

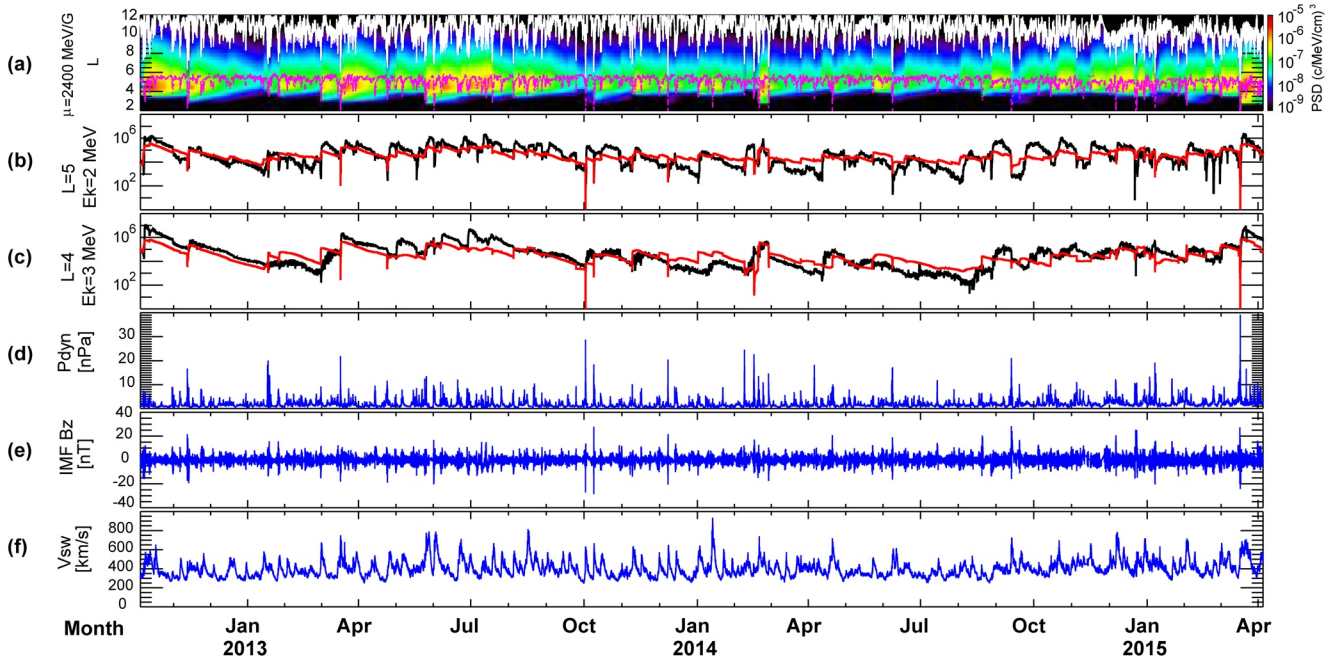

Figure 1. (a) Simulated evolution of electron PSD at $\mu = 2,400$ MeV / G as a function of L and time. The white curve shows the magnetopause position and the magenta curve indicates the plasmapause. Flux comparison between data (black curve) and model results (red curve) at (b) $L = 5$ and (c) $L = 4$. Solar wind parameters are from OMNIWeb (http://omniweb.gsfc.nasa.gov): (d) Solar wind dynamic pressure; (e) z component of interplanetary magnetic field; (f) Solar wind speed. PSD, phase space density.

assumed to follow a multivariate Gaussian. The covariance of the PE values is constructed by a Gaussian process kernel which has the property that similar sets of free parameters in the input space produce similar outputs. Then a smart choice to choose the next free parameters can be made by the acquisition function over the Gaussian prior, which is much quicker to evaluate. The acquisition functions are mathematical techniques that determine how the parameters space should be explored based on current input parameters. The scikit-optimize library was used in this study to perform the optimization (https://github.com/scikit-optimize/scikit-optimize).

3. Model Results and Discussions

We apply our model to simulate electron flux variations with equatorial pitch angle around 90° at $L = 5$ and at $L = 4$ from October 2012 to April 2015. These L values are important since $L = 4$–5 is the center of outer radiation belt with highest relativistic electron flux level. The simulation results are compared with measurements from the Van Allen Probes, which were launched into a highly elliptical and low inclination orbit on August 30, 2012 (Mauk et al., 2012). The Relativistic Electron Proton Telescope (REPT) (Baker et al., 2012) instrument onboard the Van Allen Probes provided pitch angle resolved energetic electron measurements over the critical energy range of ~2 –20 MeV. The free parameters in Equations 3–6, 9, and 11 were adjusted to get highest average PE values both at $L = 4$ and $L = 5$. Also, the linear correlation (LC) coefficients were calculated.

3.1. Long-Term Simulations

The simulation results from October 2012 to April 2015, around two and half years, are shown in Figure 1. From top to bottom, the panels show the simulated electron PSD at $\mu = 2,400$ MeV / G as a function of L and time, the comparison between simulated 2 MeV electron flux and the Van Allen Probes at $L = 5$, the comparison of 3 MeV electron flux at $L = 4$, P_{dyn}, IMF Bz, and solar wind speed. 2 MeV electrons at $L = 5$ and 3 MeV electrons at $L = 4$ share the same μ value: μ = 2,400 MeV/G. The white curve and magenta curve in panel (a) are the positions of magnetopause and plasmapause, respectively. The 2 and 3 MeV electron

Table 1
Optimum Parameter Values and Corresponding PE and LC for the Simulation Result in Figure 1

	C_1	C_2	C_3	C_4	ΔL_1	ΔL_2	ΔL_3	ΔL_4	
Values	0.25	6.5e−10	0.15	1e−3	0	0	3	3	
	γ_1	γ_2	γ_3	γ_4	γ_5	γ_6	γ_7	γ_8	γ_9
Values	1.86	0.113	0.03	1.86	1.1	0.1	0.2	1	1
	α_1	α_2	α_3	α_4		PE $_{L=5}$	LC $_{L=5}$	PE $_{L=4}$	LC $_{L=4}$
Values	70	200	70	70		0.45	0.71	0.51	0.72

LC, linear correlation; PC, prediction efficiency.

flux observations in panels (b) and (c) are interpolation results from original satellite data product since the energy channels of REPT instrument do not exactly equal 2 or 3 MeV. The model achieved a PE of 0.45 at $L = 5$ and 0.51 at $L = 4$ using the parameters listed in Table 1. The LC values at $L = 5$ and $L = 4$ are 0.71 and 0.72, respectively. The LC values in this study are calculated with original flux values. We also calculated the LC values with log fluxes. The results are higher than the LC values using original fluxes. To be consistent with the PE values, we still show the LC values using original fluxes. The electron flux experienced more variations at $L = 5$ than at $L = 4$. For example, during February 2015, 2 MeV electron flux at $L = 5$ showed some sudden decreases that are followed by a quick recovery to a high level while electron flux at $L = 4$ only showed slight variations. This phenomenon is likely due to the magnetopause shadowing and the following outward radial diffusion since electrons at $L = 5$ are closer to the magnetopause and easier to get lost. Xiang et al. (2017) suggested that, compared to the magnetopause standoff position, it is more reliable to use last closed drift shell (LCDS) to evaluate the impact of magnetopause shadowing. But, currently, there is no model to get reliable LCDS models using solar wind parameters as input. Both at $L = 5$ and at $L = 4$, the slow decay of electron fluxes inside plasmapause was well reproduced, indicating that hiss wave plays an important role in scattering the relativistic electrons into loss cones during quiet times. We also tried to tune the parameters by hand (Barker et al., 2005; Tu et al., 2009). The results are quite close to the results in Table 1 using the machine learning technique (the differences in PE are less than 0.05).

3.2. Short-Term Simulations

To investigate how much the free parameters need to be changed to predict electron fluxes better during different periods, we tuned the parameters individually to get highest PE values during every 60-days. The simulation results are shown in Figures 2a–2c while two short-term simulation results are shown in Figures 2d–2i (corresponding to the first 60-days in Figures 2a) and Figures 2j–2o (corresponding to the last 60-days in Figure 2a), respectively. The model achieved a PE of 0.58 at $L = 5$ and 0.82 at $L = 4$ for the two and half years using the parameters listed in Table 2. The LC values at $L = 5$ and $L = 4$ are 0.77 and 0.91, respectively. The values of $\gamma_1 - \gamma_9$, $\alpha_1 - \alpha_4$ are kept same as those in Table 1 to focus on improving the model results by only tuning parameters listed in Table 2. For these free parameters, C_1–C_4 are scaling factors and ΔL_1–ΔL_4 are space width factors. These eight parameters have their assigned physical meanings. Thus, we only tune these eight parameters in this section. This will also reduce the CPU operation time. To ensure the physical reasonability of free parameters, the value of free parameters can only be adjusted in predefined ranges. Mostly, the ranges of scaling factors are one order larger/smaller than empirical values. The optimized free parameters in Table 2 mainly show physically reasonable values. For example, the residual standard deviation of the plasmapause model in Verbanac et al. (2015) is 0.86. The space width factors ΔL_2 in Table 2 are mostly smaller than 0.86, suggesting that the values of ΔL_2 are physically reasonable. Compared to the long-term simulation results in Figure 1, the model gets much higher PE values at both $L = 4$ and $L = 5$ using time updated parameters. Especially for $L = 4$, the PE values significantly increase from 0.51 to 0.82. It can be observed that in panel (f) and panel (l) the simulation results mostly reproduced the actual variations of electron fluxes at $L = 4$. In contrast, some decreases of electron flux at $L = 5$ (see panel k) are still not well captured by the model. These decreases of 2 MeV electron flux at $L = 5$ are all accompanied with decreases of magnetopause position, indicating that the loss due to magnetopause shadowing is not

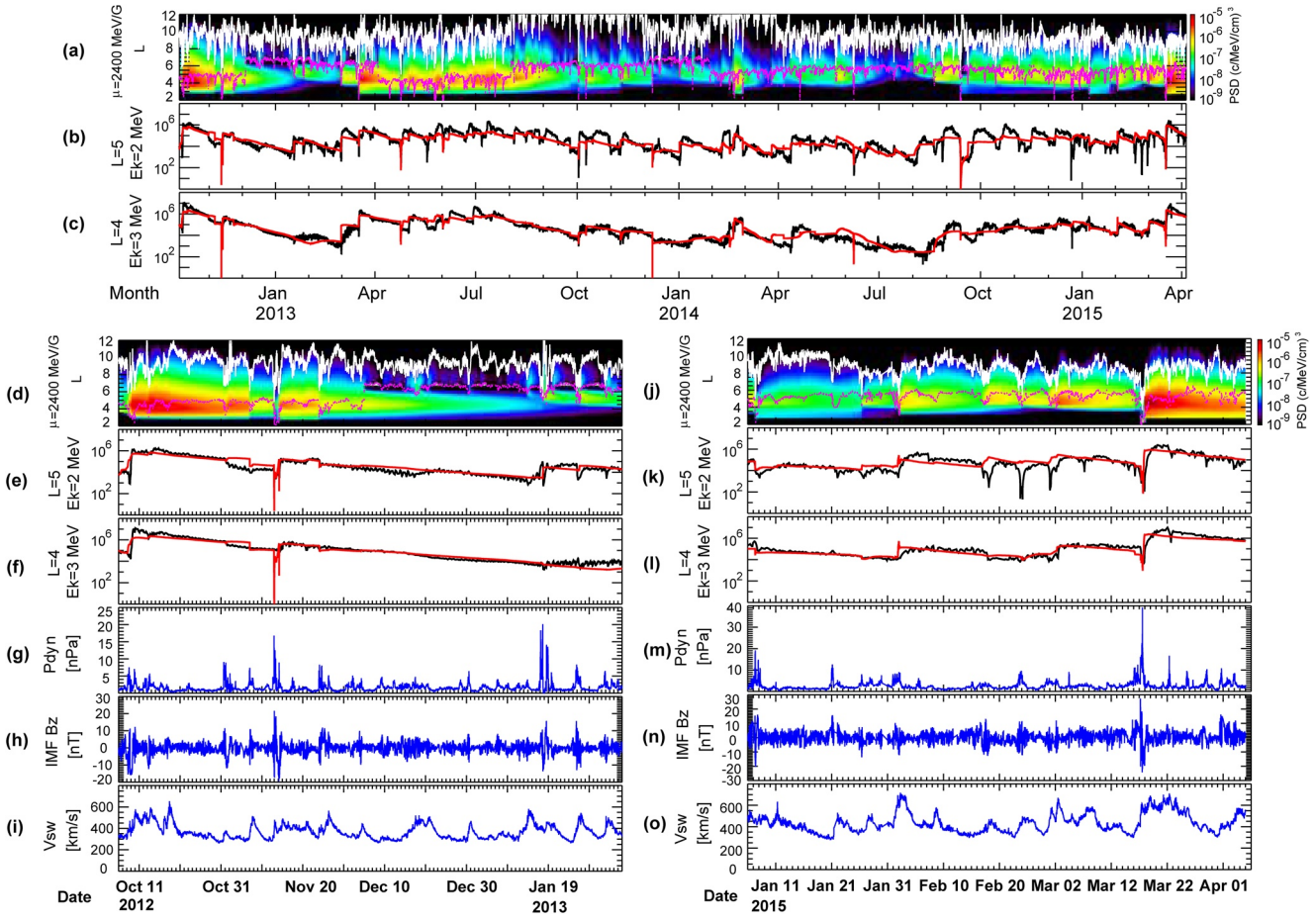

Figure 2. (a)–(c) Same format as Figures 1a–1c but for free parameters updated every 2 months. (d)–(e) Same format as Figures 1a–1c but for October 2012–January 2013 using different free parameters. (j)–(o) Same format as panels (d)–(e) but for January–April 2015.

well captured in our model. In Table 2, the parameters have very different values in different periods, suggesting that we may need to express some parameters as functions to account for these differences. We also plot these optimum parameter values as time series and show the results in Figure 3. The left panel shows free parameter values in Table 2 as a function of time periods while the right panel shows free parameter values normalized to parameter values during period 1. It is clear to see that there are two free parameters (C_3, C_4) with large variations. The two parameters are used to adjust $h(Kp)$ and quick loss due to EMIC waves using a similar formula for radial diffusion rate. The large variations in the two parameters suggest that the formula for radial diffusion is not a good choice to represent $h(Kp)$ and loss due to EMIC, which should be improved in the future studies.

3.3. Simulations With Free Parameters Adjusted by Solar Wind Parameters

The above section has demonstrated that using time-updated parameters can get higher PE values. Therefore, in this section, we try to use different set of parameters based on the solar wind conditions in the model to get better simulation results. Generally, we divide solar wind parameters into three categories to represent active, moderate, and quiet periods, respectively. Figure 4 shows three cases of simulation results with parameters adjusted by the solar wind speed (Figures 4a–4c), IMF Bz (Figures 4d–4f) and solar wind dynamic pressure (Figures 4g–4i), respectively. The solar wind speed is divided into three categories: $v < 400$ km/s, 400 km/s $< v <$ 600 km/s, $v >$ 600 km/s . Corresponding to each category of solar wind speed, a set of parameters $(C_1 - C_4, \Delta L_1 - \Delta L_4)$ are used, namely three sets of parameters are tuned in the model to

Table 2
Optimum Parameter Values and Corresponding PE and LC for the Simulation Result in Figure 2

Period	C_1	$C_2 \times 10^{10}$	C_3	$C_4 \times 10^3$	ΔL_1	ΔL_2	ΔL_3	ΔL_4
1	0.95	14.4	0.39	0.1	−1.5	−0.57	3.13	2
2	0.11	20	0.22	8.7	−1.5	1.22	4.99	2
3	0.19	8.87	0.32	20	−1.5	0.85	2	3.36
4	1.8	10.94	3.39	0.46	−1.5	−1.13	2	5
5	0.88	5	0.47	4.48	−1.5	−0.63	4.9	5
6	0.11	20	0.30	1.57	1.5	0.79	2.2	2.67
7	0.35	6.44	0.39	2.83	1.03	0.63	5	3.52
8	0.17	15.39	4.38	0.29	−1.5	1.31	3.36	2
9	0.86	5	0.1	2.15	1.03	−0.09	5	4.88
10	0.54	10.18	10	0.65	−1.5	0.33	5	3.84
11	0.49	7.28	0.1	0.29	−1.5	0.37	2.44	2.75
12	0.11	20	0.67	0.79	−1.48	0.7	2	5
13	0.23	8.42	6.12	2.8	−1.5	0.41	2.19	3.22
14	0.48	5	0.36	5.02	−0.9	0.23	2.95	2.45
15	0.35	18.6	0.11	1.44	−1.5	0.51	4	4.35
16	1.03	5	1.88	7.22	−1.13	0.79	2.81	3.6
	$PE_{L=5}$	$LC_{L=5}$	$PE_{L=4}$	$LC_{L=4}$				
Values	0.58	0.77	0.82	0.91				

LC, linear correlation; PC, prediction efficiency.

get best simulation results. The parameters for the three solar wind speed categories are shown in Table 3. The model achieved a PE of 0.54 at $L = 5$ and 0.58 at $L = 4$. The LC values at $L = 5$ and $L = 4$ are 0.75 and 0.77, respectively. These simulation results are not as good as the results in Section 3.2, but are better than using the one set of parameters for the whole period. Similarly, IMF Bz is divided into three categories: $Bz < -3\,nT, -3\,nT < Bz < 0\,nT, Bz > 0\,nT$. The model achieved a PE of 0.45 at $L = 5$ and 0.53 at $L = 4$. The

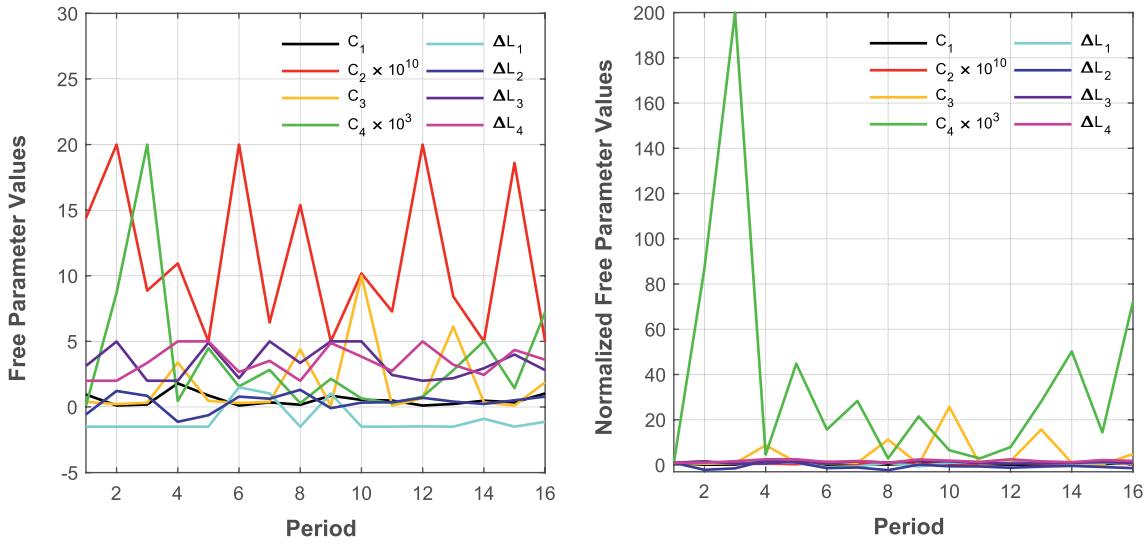

Figure 3. (a) Free parameter values and (b) Normalized free parameter values in Table 2 as a function of time period. The normalized values are obtained by dividing free parameter values during period 1.

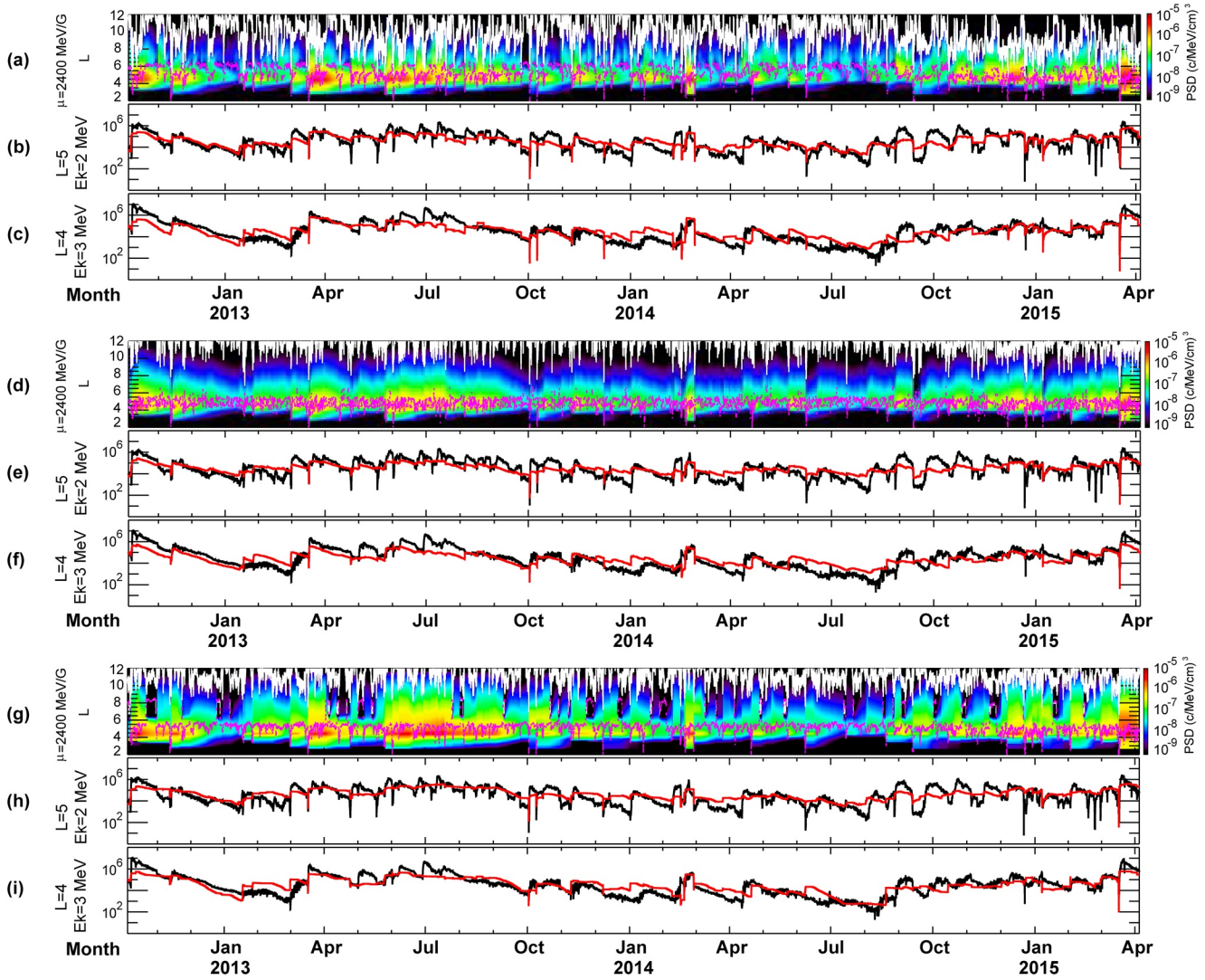

Figure 4. Same format as Figures 1a–1c but using parameters adjusted by solar wind speed (a–c), by IMF Bz (d–f), and by P_{dyn} (g–i). IMF, interplanetary magnetic field.

LC values at $L = 5$ and $L = 4$ are 0.72 and 0.75, respectively. The PE values and LC values are almost the same as results in Figure 1, suggesting that it is better to change the set of parameters by solar wind speed, which seems to have the most influence on the variations of the MeV electrons inside magnetosphere. In Figures 4g–4i, the model achieved a PE of 0.46 at $L = 5$ and 0.62 at $L = 4$ by dividing P_{dyn} into three categories: $P_{dyn} < 3$ nPa, 3 nPa $< P_{dyn} < 6$ nPa, $P_{dyn} > 6$ nPa. The PE value (0.62) at $L = 4$ is the highest of the three cases in Figure 4, indicating that P_{dyn} has an important influence on electrons at $L = 4$. In contrast, the PE value (0.46) at $L = 5$ is close to the result (PE = 0.45) under three IMF Bz conditions and lower than the PE value (0.54) obtained under three solar wind speed conditions. It seems that the electron fluxes at higher L have closer relationship with solar wind speed, which is consistent with conclusions in previous studies (e.g., Li et al., 2001) that the solar wind speed is the most important parameter governing relativistic electron fluxes at the geostationary orbit. Some studies pointed out that IMF Bz plays important roles in both electron loss and acceleration (Li et al., 2015; Ni et al., 2016). However, it is unclear in this study why the treatment to divide IMF Bz into three categories only slightly improves PE values.

Over the past, we have developed several models to predict and analyze the electron flux in the inner magnetosphere. The first model we developed used radial diffusion to model the electron flux at GEO orbit. The

Table 3
Optimum Parameter Values and Corresponding PE and LC for the Simulation Result in Figure 4

Vsw (km/s) condition	C_1	$C_2 \times 10^{10}$	C_3	$C_4 \times 10^3$	ΔL_1	ΔL_2	ΔL_3	ΔL_4
<400	0.11	18.9	0.1	19.98	0.49	0.67	4.38	4.88
(400, 600)	0.09	3.15	0.81	0.76	−1.98	−0.29	3.98	2
>600	0.01	10.58	0.33	1.37	−0.58	−0.06	5.06	4.64
	$PE_{L=5}$	$LC_{L=5}$	$PE_{L=4}$	$LC_{L=4}$				
Values	0.54	0.75	0.58	0.77				
Bz (nT) condition	C_1	$C_2 \times 10^{10}$	C_3	$C_4 \times 10^3$	ΔL_1	ΔL_2	ΔL_3	ΔL_4
<−3	0.21	5	0.13	1.89	1.5	−0.1	3.35	8
(−3, 0)	0.43	5	0.13	20	2	−1	4.67	5
>0	0.08	19	8.88	20	−0.89	1	2	5
	$PE_{L=5}$	$LC_{L=5}$	$PE_{L=4}$	$LC_{L=4}$				
Values	0.45	0.72	0.53	0.75				
Pdyn (nPa) condition	C_1	$C_2 \times 10^{10}$	C_3	$C_4 \times 10^3$	ΔL_1	ΔL_2	ΔL_3	ΔL_4
<3	0.2	11.7	0.50	18.4	−0.52	2.82	3.8	4.38
(3, 6)	0.13	2	0.1	7.5	0.06	−0.01	3.01	2.88
>6	0.004	5	2.4	2.2	1.48	−0.06	7.34	3.72
	$PE_{L=5}$	$LC_{L=5}$	$PE_{L=4}$	$LC_{L=4}$				
Values	0.46	0.71	0.62	0.79				

LC, linear correlation; PC, prediction efficiency.

model uses the Fokker-Plank equation with the diffusion coefficient a function of solar wind parameters (Li, 2004; Li et al., 2001). This model reproduces well the MeV electron flux at GEO, achieving a prediction efficiency (PE) of the log of electron flux of 0.81 and a linear correlation of 0.9 for the years 1995–1996 based on comparison with daily-averaged LANL 0.7–1.8 MeV electron data at GEO. A version of this model is also running 24/7 using real-time solar wind data (https://lasp.colorado.edu/home/personnel/xinlin.li/) to forecast the electron flux one and two days ahead. This model was extended to allow for comparison with measurements at more than one L while retaining a similar form for the diffusion coefficient (Barker et al., 2005). The extended model achieved a PE of 0.61 at $L = 4$ and 0.52 at $L = 6$ when compared with orbit averaged 2 MeV electron fluxes measured by Polar satellite at $L = 4$ and the daily averaged LANL 0.7–1.8 MeV electron fluxes measured at GEO for the year of 1998. A second model using low energy (~50 keV) electrons to predict higher energy (~1 MeV) electrons at GEO 1–2 days ahead showed good accuracy (Turner & Li, 2008) and quantified the systematic hardening of the electron spectrum. This model, in contrast to the radial diffusion model, suggests that the radiation belts can be formed by the injection of lower energy electrons from the magnetotail which then hardened (i.e., accelerated by chorus waves) to form the radiation belt. A third model, also one-dimensional, Tu et al. (2009) incorporated radial diffusion, loss and a source term to model the relativistic electron flux for a range of L values inside GEO using data at geosynchronous orbit as a boundary condition for energies corresponding to a single value of the first adiabatic invariant, μ. The model can be made to work well for individual storms but is difficult because of the needed adjustment of parameters for each storm and because the source term doses not properly model heating. From developing this model, we also learned that radial diffusion alone is not sufficient to reproduce the electron flux and that for many storms an additional heating term is required. Thus, in this study, we build a model incorporating the local heating term and loss mechanisms driven by solar wind parameters to reproduce electron flux variations.

4. Summary

In this study, we have established a 1-D radial diffusion model incorporating internal source and loss terms to simulate the radiation belt electron flux variations at $L = 5$ and at $L = 4$ from October 2012 to April 2015. Different from previous studies (e.g., Tu et al., 2009), the source and loss terms in our model are all related to solar wind parameters rather than geomagnetic indices and our model is also applied for a longer period. We have considered PSD data at $\mu = 2,400$ MeV / G corresponding to 2 MeV electrons at $L = 5$ and corresponding to 3 MeV electrons at $L = 4$. The long-term simulation results have overall reproduced the observations of radiation belt electron flux variation but with certain over-prediction and under-prediction at different time intervals, suggesting that the same set of parameters cannot be applied to the whole simulation period based on our 1-D model. Therefore, the simulations using parameters tuned by different periods and different solar wind conditions have been conducted to obtain higher PE values (shown in Figures 2 and 4). These results demonstrate that using different sets of parameters for different periods is another method to get better simulation results. We have also found that P_{dyn} plays an important role in governing relativistic electron fluxes at lower L (e.g., $L = 4$) while solar wind speed is the dominant factor affecting relativistic electron fluxes at higher L (e.g., $L = 5$). Several previous studies have investigated the relationships between electron flux variations and solar wind conditions. Using the electron flux data measured by POES and GOES satellites, Ni et al. (2016) investigated the flux variations of energetic electrons during solar wind dynamic pressure pulses and found that the pressure pulses with longer durations tend to produce quicker and stronger electron flux decay. By performing superposed epoch analysis of solar wind parameters during efficient and inefficient acceleration events, Li et al. (2015) shown that prolonged southward Bz, high solar wind speed, and low dynamic pressure are important for >1 MeV electron accelerations. However, the preferred solar wind parameters for electron increase and decrease at different L values have not been fully investigated, which we leave for further studies.

Generally, the simulation results at $L = 4$ are better than those at $L = 5$. A likely explanation can be that the magnetopause shadowing effect is not well included in our model. To improve our model performance, it will be better to use the LCDS rather than magnetopause standoff position in the model. To reduce the CPU operation time, only values of $\gamma_1 - \gamma_9$, $\alpha_1 - \alpha_4$ are tuned, as described in Sections 3.2 and 3.3. Although the simulation period October 2012–April 2015 in this study is during the solar maximum of solar cycle 24, the geomagnetic activities during the year 2014 were relatively low and radiation belt electron flux experienced unusually low level (L. Y. Li et al., 2017). Our model well reproduced the low electron flux level during October 2013–September 2014 as observed in Figures 1a and 2a, suggesting that our model can be used during both active and quiet periods.

Data Availability Statement

All Van Allen Probes ECT/REPT Level-3 data are available at www.rbsp-ect.lanl.gov. The solar wind parameters used in this study are obtained from the OMNIWeb database (http://omniweb.gsfc.nasa.gov). The model codes can be found at https://doi.org/10.6084/m9.figshare.14269127.v1.

Acknowledgments
This work was supported by the NSF Grant (AGS 1834971), NASA grants (NNX17AD85G and NSSC19K0237). Z. Xiang thanks the support from the NSFC Grants (41904143 and 42025404), the Fundamental Research Funds for the Central Universities 2042021kf0016, and the China Postdoctoral Science Foundation project 2019M662700. B. Ni thanks the support from the preresearch projects on Civil Aerospace Technologies No. D020308 funded by the China National Space Administration.

References

Abel, B., & Thorne, R. M. (1998). Electron scattering loss in Earth's inner magnetosphere: 1. Dominant physical processes. *Journal of Geophysical Research*, *103*(A2), 2385–2396. https://doi.org/10.1029/97JA02919

Baker, D. N. (2001). Satellite anomalies due to space storms. In *Space storms and space weather hazards* (pp. 285–311). Springer. https://doi.org/10.1007/978-94-010-0983-6_11

Baker, D. N., Allen, J. H., Kanekal, S. G., & Reeves, G. D. (1998). Disturbed space environment may have been related to pager satellite failure. *Eos, Transactions, American Geophysical Union*, *79*(40), 477. https://doi.org/10.1029/98EO00359

Baker, D. N., Kanekal, S. G., Hoxie, V. C., Batiste, S., Bolton, M., Li, X., et al. (2012). The relativistic electron-proton telescope (REPT) instrument on board the radiation belt storm probes (RBSP) spacecraft: Characterization of Earth's radiation belt high-energy particle populations. *Space Science Reviews*, *179*, 337–381. https://doi.org/10.1007/s11214-012-9950-9

Baker, D. N., Pulkkinen, T. I., Li, X., Kanekal, S. G., Blake, J. B., Selesnick, R. S., et al. (1998). Coronal mass ejections, magnetic clouds, and relativistic magnetospheric electron events: ISTP. *Journal of Geophysical Research*, *103*, 17279–17291. https://doi.org/10.1029/97JA03329

Balikhin, M. A., Boynton, R. J., Walker, S. N., Borovsky, J. E., Billings, S. A., & Wei, H. L. (2011). Using the NARMAX approach to model the evolution of energetic electrons fluxes at geostationary orbit. *Geophysical Research Letters*, *38*, L18105. https://doi.org/10.1029/2011GL048980

Balikhin, M. A., Rodriguez, J. V., Boynton, R. J., Walker, S. N., Aryan, H., Sibeck, D. G., & Billings, S. A. (2016). Comparative analysis of NOAA REFM and SNB3GEO tools for the forecast of the fluxes of high-energy electrons at GEO. *Space Weather*, *14*, 22–31. https://doi.org/10.1002/2015SW001303

Barker, A. B., Li, X., & Selesnick, R. S. (2005). Modeling the radiation belt electrons with radial diffusion driven by the solar wind. *Journal of Geophysical Research*, *3*, S10003. https://doi.org/10.1029/2004SW000118

Blum, L. W., Halford, A., Millan, R., Bonnell, J. W., Goldstein, J., Usanova, M., et al. (2015). Observations of coincident EMIC wave activity and duskside energetic electron precipitation on 18–19 January 2013. *Geophysical Research Letters*, *42*, 5727–5735. https://doi.org/10.1002/2015GL065245

Boyd, A. J., Turner, D. L., Reeves, G. D., Spence, H. E., Baker, D. N., & Blake, J. B. (2018). What causes radiation belt enhancements: A survey of the Van Allen Probes Era. *Geophysical Research Letters*, *45*, 5253–5259. https://doi.org/10.1029/2018GL077699

Boynton, R. J., Balikhin, M. A., Billings, S. A., Reeves, G. D., Ganushkina, N., Gedalin, M., et al. (2013). The analysis of electron fluxes at geosynchronous orbit employing a NARMAX approach. *Journal of Geophysical Research: Space Physics*, *118*, 1500–1513. https://doi.org/10.1002/jgra.50192

Boynton, R. J., Balikhin, M. A., Sibeck, D. G., Walker, S. N., Billings, S. A., & Ganushkina, N. (2016). Electron flux models for different energies at geostationary orbit. *Journal of Geophysical Research: Space Weather*, *14*, 846–860. https://doi.org/10.1002/2016SW001506

Breneman, A. W., Halford, A., Millan, R., McCarthy, M., Fennell, J., Sample, J., et al. (2015). Global-scale coherence modulation of radiation-belt electron loss from plasmaspheric hiss. *Nature*, *523*, 193–195. https://doi.org/10.1038/nature14515

Chen, H., Gao, X., Lu, Q., Tsurutani, B. T., & Wang, S. (2020). Statistical evidence for EMIC wave excitation driven by substorm injection and enhanced solar wind pressure in the Earth's magnetosphere: Two different EMIC wave sources. *Geophysical Research Letters*, *47*, e2020GL090275. https://doi.org/10.1029/2020GL090275

Chen, Y., Reeves, G. D., & Friedel, R. H. W. (2007). The energization of relativistic electrons in the outer Van Allen radiation belt. *Nature Physics*, *3*(9), 614–617. https://doi.org/10.1038/nphys655

Fennell, J. F., Koons, H. C., Roeder, J. L., & Blake, J. B. (2001). *Spacecraft charging: Observations and relationship to satellite anomalies* (pp. 279–285). Europe Space Agency Special Publications. https://doi.org/10.10101/esasp825433

Frazier, P. (2018). *A tutorial on Bayesian optimization*. Retrieved from https://arxiv.org/pdf/1807.02811

Fu, S., Yi, J., Ni, B., Zhou, R., Hu, Z., Cao, X., et al. (2020). Combined scattering of radiation belt electrons by low-frequency hiss: Cyclotron, landau, and bounce resonances. *Geophysical Research Letters*, *47*, e2020GL086963. https://doi.org/10.1029/2020GL086963

Horne, R. B., Thorne, R. M., Shprits, Y. Y., Meredith, N. P., Glauert, S. A., Smith, A. J., et al. (2005). Wave acceleration of electrons in the Van Allen radiation belts. *Nature*, *437*(7056), 227–230. https://doi.org/10.1038/nature03939

Jaynes, A. N., Baker, D. N., Singer, H. J., Rodriguez, J. V., Loto'aniu, T. M., Ali, A. F., et al. (2015). Source and seed populations for relativistic electrons: Their roles in radiation belt changes. *Journal of Geophysical Research: Space Physics*, *120*, 7240–7254. https://doi.org/10.1002/2015JA021234

Ji, E.-Y., Moon, Y.-J., Park, J., Lee, J.-Y., & Lee, D.-H. (2013). Comparison of neural network and support vector machine methods for Kp forecasting. *Journal of Geophysical Research: Space Physics*, *118*, 5109–5117. https://doi.org/10.1002/jgra.50500

Lessard, M. R., Paulson, K., Spence, H. E., Weaver, C., Engebretson, M. J., Millan, R., et al. (2019). Generation of EMIC waves and effects on particle precipitation during a solar wind pressure intensification with B z >0. *Journal of Geophysical Research: Space Physics*, *124*, 4492–4508. https://doi.org/10.1029/2019JA026477

Li, L. Y., Cao, J. B., Zhou, G. C., & Li, X. (2009). Statistical roles of storms and substorms in changing the entire outer zone relativistic electron population. *Journal of Geophysical Research*, *114*, A1221. https://doi.org/10.1029/2009JA014333

Li, L. Y., Yu, J., Cao, J. B., Yang, J. Y., Li, X., Baker, D. N., et al. (2017). Roles of whistler mode waves and magnetosonic waves in changing the outer radiation belt and the slot region. *Journal of Geophysical Research: Space Physics*, *122*, 5431–5448. https://doi.org/10.1002/2016JA023634

Li, W., Thorne, R. M., Bortnik, J., Baker, D. N., Reeves, G. D., Kanekal, S. G., et al. (2015). Solar wind conditions leading to efficient radiation belt electron acceleration: A superposed epoch analysis. *Geophysical Research Letters*, *42*, 6906–6915. https://doi.org/10.1002/2015GL065342

Li, X. (2004). Variations of 0.7-6.0 MeV electrons at geosynchronous orbit as a function of solar wind. *Journal of Geophysical Research Space Weather*, *2*, S03006. https://doi.org/10.1029/2003SW000017

Li, X., Baker, D. N., O'Brien, T. P., Xie, L., & Zong, Q. G. (2006). Correlation between the inner edge of outer radiation belt electrons and the innermost plasmapause location. *Geophysical Research Letters*, *33*, L14107. https://doi.org/10.1029/2006GL026294

Li, X., Baker, D. N., Temerin, M., Cayton, T. E., Reeves, E. G. D., Christensen, R. A., et al. (1997). Multisatellite observations of the outer zone electron variation during the November 3–4, 1993, magnetic storm. *Journal of Geophysical Research*, *102*, 14123–14140. https://doi.org/10.1029/97JA01101

Li, X., Baker, D. N., Teremin, M., Cayton, T. E., Reeves, G. D., Selesnick, R. S., et al. (1999). Rapid enchancements of relativistic electrons deep in the magnetosphere during the May 15, 1997, magnetic storm. *Journal of Geophysical Research*, *104*(A4), 4467–4476. https://doi.org/10.1029/1998JA900092

Li, X., Baker, D. N., Zhao, H., Zhang, K., Jaynes, A. N., Schiller, Q., et al. (2017). Radiation belt electron dynamics at low L. *Journal of Geophysical Research: Space Physics*, *122*, 5224–5234. https://doi.org/10.1002/2017JA023924

Li, X., Temerin, M., Baker, D. N., & Reeves, G. D. (2011). Behavior of MeV electrons at geosynchronous orbit during last two solar cycles. *Journal of Geophysical Research*, *116*, A11207. https://doi.org/10.1029/2011JA016934

Li, X., Temerin, M., Baker, D. N., Reeves, G. D., & Larson, D. (2001). Quantitative prediction of radiation belt electrons at geostationary orbit based on solar wind measurements. *Geophysical Research Letters*, *28*(9), 1887–1890. https://doi.org/10.1029/2000GL012681

Mauk, B. H., Fox, N. J., Kanekal, S. G., Kessel, R. L., Sibeck, D. G., & Ukhorskiy, A. (2012). Science objectives and rationale for the Radiation Belt Storm Probes mission. *Space Science Reviews*, *179*, 3–27. https://doi.org/10.1007/s11214-012-9908-y

Ma, X., Xiang, Z., Xiang, Z., Ni, B., Fu, S., Cao, X., et al. (2020). On the loss mechanisms of radiation belt electron dropouts during the 12 September 2014 geomagnetic storm. *Earth and Planetary Physics*, *4*(6), 1–13. https://doi.org/10.26464/epp2020060

Morley, S. K., Friedel, R. H. W., Cayton, T. E., & Noveroske, E. (2010). A rapid, global and prolonged electron radiation belt dropout observed with the Global Positioning System constellation. *Geophysical Research Letters*, *37*, L06102. https://doi.org/10.1029/2010GL042772

Ni, B., Bortnik, J., Thorne, R. M., Ma, Q., & Chen, L. (2013). Resonant scattering and resultant pitch angle evolution of relativistic electrons by plasmaspheric hiss. *Journal of Geophysical Research: Space Physics*, *118*, 7740–7751. https://doi.org/10.1002/2013JA019260

Ni, B., Cao, X., Zou, Z., Zhou, C., Gu, X., Bortnik, J., et al. (2015). Resonant scattering of outer zone relativistic electrons by multiband EMIC waves and resultant electron loss time scales. *Journal of Geophysical Research: Space Physics*, *120*, 7357–7373. https://doi.org/10.1002/2015JA021466

Ni, B., Hua, M., Zhou, R., Yi, J., & Fu, S. (2017). Competition between outer zone electron scattering by plasmaspheric hiss and magnetosonic waves. *Geophysical Research Letters*, *44*, 3465–3474. https://doi.org/10.1002/2017GL072989

Ni, B., Huang, H., Zhang, W., Gu, X., Zhao, H., Li, X., et al. (2019). Parametric sensitivity of the formation of reversed electron energy spectrum caused by plasmaspheric hiss. *Geophysical Research Letters*, *46*, 4134–4143. https://doi.org/10.1029/2019GL082032

Ni, B., Thorne, R. M., Meredith, N. P., Shprits, Y. Y., & Horne, R. B. (2011). Diffuse auroral scattering by whistler mode chorus waves: Dependence on wave normal angle distribution. *Journal of Geophysical Research*, *116*, A10207. https://doi.org/10.1029/2011JA016517

Ni, B., Thorne, R. M., Shprits, Y. Y., & Bortnik, J. (2008). Resonant scattering of plasma sheet electrons by whistler-mode chorus: Contribution to diffuse auroral precipitation. *Geophysical Research Letters*, *35*, L11106. https://doi.org/10.1029/2008GL034032

Ni, B., Xiang, Z., Gu, X., Shprits, Y. Y., Zhou, C., Zhao, Z., et al. (2016). Dynamic responses of the Earth's radiation belts during periods of solar wind dynamic pressure pulse based on normalized superposed epoch analysis. *Journal of Geophysical Research: Space Physics*, *121*, 8523–8536. https://doi.org/10.1002/2016JA023067

Orlova, K., Shprits, Y., & Spasojevic, M. (2016). New global loss model of energetic and relativistic electrons based on Van Allen Probes measurements. *Journal of Geophysical Research: Space Physics*, *121*, 1308–1314. https://doi.org/10.1002/2015JA021878

Paulikas, G. A., & Blake, J. B. (1979). Effects of the solar wind on magnetospheric dynamics: Energetic electrons at the synchronous orbit. In W. P. Olson (Ed.), *Quantitative modeling of magnetospheric processes, Geophysical monograph series* (pp. 180–202). American Geophysical Union. https://doi.org/10.1029/GM021p0180

Rasmussen, C. E., & Nickisch, H. (2010). Gaussian processes for machine learning (gpml) toolbox. *Journal of Machine Learning Research*, *11*(6), 3011–3015. https://doi.org/10.1115/1.4002474

Reeves, G. D., Morley, S. K., Friedel, R. H. W., Henderson, M. G., Cayton, T. E., Cunningham, G., et al. (2011). On the relationship between relativistic electron flux and solar wind velocity: Paulikas and Blake revisited. *Journal of Geophysical Research*, *116*, A02213. https://doi.org/10.1029/2010JA015735

Reeves, G. D., Spence, H. E., Henderson, M. G., Morley, S. K., Friedel, R. H. W., Funsten, H. O., et al. (2013). Electron acceleration in the heart of the Van Allen radiation belts. *Science*, *341*(6149), 991–994. https://doi.org/10.1126/science.1237743

Saikin, A. A., Zhang, J.-C., Smith, C. W., Spence, H. E., Torbert, R. B., & Kletzing, C. A. (2016). The dependence on geomagnetic conditions and solar wind dynamic pressure of the spatial distributions of emic waves observed by the Van Allen Probes. *Journal of Geophysical Research: Space Physics*, *121*, 4362–4377. https://doi.org/10.1002/2016JA022523

Schulz, M., & Lanzerotti, L. J. (1974). Particle diffusion in the radiation belts. In *Physics and Chemistry in Space* (Vol. 7). Springer.

Shprits, Y. Y., Thorne, R. M., Friedel, R., Reeves, G. D., Fennell, J., Baker, D. N., & Kanekal, S. G. (2006). Outward radial diffusion driven by losses at magnetopause. *Journal of Geophysical Research*, *111*, A11214. https://doi.org/10.1029/2006JA011657

Shprits, Y. Y., Thorne, R. M., Horne, R. B., Glauert, S. A., Cartwright, M., Russell, C. T., et al. (2006). Acceleration mechanism responsible for the formation of the new radiation belt during the 2003 Halloween solar storm. *Geophysical Research Letters*, *33*, L05104. https://doi.org/10.1029/2005GL024256

Shue, J.-H., Song, P., Russell, C. T., Steinberg, J. T., Chao, J. K., Zastenker, G., et al. (1998). Magnetopause location under extreme solar wind conditions. *Journal of Geophysical Research*, *103*(A8), 17691–17700. https://doi.org/10.1029/98JA01103

Summers, D., Ni, B., & Meredith, N. P. (2007). Timescales for radiation belt electron acceleration and loss due to resonant wave-particle interactions: 1. Theory. *Journal of Geophysical Research*, *112*, A04206. https://doi.org/10.1029/2006JA011801

Thorne, R. M. (2010). Radiation belt dynamics: The importance of wave-particle interactions. *Geophysical Research Letters*, *37*, L22107. https://doi.org/10.1029/2010GL044990

Turner, D. L., Angelopoulos, V., Li, W., Bortnik, J., Ni, B., Ma, Q., et al. (2014). Competing source and loss mechanisms due to wave-particle interactions in Earth's outer radiation belt during the 30 September to 3 October 2012 geomagnetic storm. *Journal of Geophysical Research: Space Physics*, *119*, 1960–1979. https://doi.org/10.1002/2014JA019770

Turner, D. L., & Li, X. (2008). Quantitative forecast of relativistic electron flux at geosynchronous orbit based on low-energy electron flux. *Journal of Geophysical Research: Space Weather*, *6*, S05005. https://doi.org/10.1029/2007SW000354

Turner, D. L., Shprits, Y., Hartinger, M., & Angelopoulos, V. (2012). Explaining sudden losses of outer radiation belt electrons during geomagnetic storms. *Nature Physics*, *8*, 208–212. https://doi.org/10.1038/nphys2185

Tu, W., Li, X., Chen, Y., Reeves, G. D., & Temerin, M. (2009). Storm-dependent radiation belt electron dynamics. *Journal of Geophysical Research*, *114*, A02217. https://doi.org/10.1029/2008JA013480

Tu, W., Selesnick, R., Li, X., & Looper, M. (2010). Quantification of the precipitation loss of radiation belt electrons observed by SAMPEX. *Journal of Geophysical Research*, *115*, A07210. https://doi.org/10.1029/2009JA014949

Verbanac, G., Pierrard, V., Bandić, M., Darrouzet, F., Rauch, J.-L., & Décréau, P. (2015). The relationship between plasmapause, solar wind and geomagnetic activity between 2007 and 2011. *Annals of Geophysics*, *33*, 1271–1283. https://doi.org/10.5194/angeo-33-1271-2015

Wing, S., Johnson, J. R., Jen, J., Meng, C.-I., Sibeck, D. G., Bechtold, K., et al. (2005). Kp forecast models. *Journal of Geophysical Research*, *110*, A04203. https://doi.org/10.1029/2004JA010500

Xiang, Z., Ni, B., Zhou, C., Zou, Z., Gu, X., Zhao, Z., et al. (2016). Multi-satellite simultaneous observations of magnetopause and atmospheric losses of radiation belt electrons during an intense solar wind dynamic pressure pulse. *Annals of Geophysics*, *34*(5), 493–509. https://doi.org/10.5194/angeo-34-493-2016

Xiang, Z., Tu, W., Li, X., Ni, B., Morley, S. K., & Baker, D. N. (2017). Understanding the mechanisms of radiation belt dropouts observed by Van Allen Probes. *Journal of Geophysical Research: Space Physics*, *122*, 9858–9879. https://doi.org/10.1002/2017JA024487

Xiang, Z., Tu, W., Ni, B., Henderson, M. G., & Cao, X. (2018). A statistical survey of radiation belt dropouts observed by Van Allen Probes. *Geophysical Research Letters*, *45*, 8035–8043. https://doi.org/10.1029/2018GL078907

Zhang, W., Fu, S., Gu, X., Ni, B., Xiang, Z., Summers, D., et al. (2018). Electron scattering by plasmaspheric hiss in a nightside plume. *Geophysical Research Letters*, *45*, 4618–4627. https://doi.org/10.1029/2018GL077212

Zhang, W., Ni, B., Huang, H., Summers, D., Fu, S., Xiang, Z., et al. (2019). Statistical properties of hiss in plasmaspheric plumes and associated scattering losses of radiation belt electrons. *Geophysical Research Letters*, *46*, 5670–5680. https://doi.org/10.1029/2018GL081863

Zhao, H., Baker, D. N., Li, X., Jaynes, A. N., & Kanekal, S. G. (2019). The effects of geomagnetic storms and solar wind conditions on the ultrarelativistic electron flux enhancements. *Journal of Geophysical Research: Space Physics*, *124*, 1948–1965. https://doi.org/10.1029/2018JA026257

Zhao, H., Friedel, R. H. W., Chen, Y., Reeves, G. D., Baker, D. N., Li, X., et al. (2018). An empirical model of radiation belt electron pitch angle distributions based on Van Allen Probes measurements. *Journal of Geophysical Research: Space Physics*, *123*, 3493–3511. https://doi.org/10.1029/2018JA025277

Zhao, H., Johnston, W. R., Baker, D. N., Li, X., Ni, B., Jaynes, A. N., et al. (2019). Characterization and evolution of radiation belt electron energy spectra based on the Van Allen Probes measurements. *Journal of Geophysical Research: Space Physics*, *124*, 4217–4232. https://doi.org/10.1029/2019JA026697

Zhao, H., & Li, X. (2013). Modeling energetic electron penetration into the slot region and inner radiation belt. *Journal of Geophysical Research: Space Physics*, *118*, 6936–6945. https://doi.org/10.1002/2013JA019240

Zhao, H., Ni, B., Li, X., Baker, D. N., Johnston, W. R., Zhang, W., et al. (2019). Plasmaspheric hiss waves generate a reversed energy spectrum of radiation belt electrons. *Nature Physics*, *15*, 367–372. https://doi.org/10.1038/s41567-018-0391-6